ONE EIGHTH OF A SPHERE MICROPHONE ARRAY

Pierre Lecomte[1]   **Torea Blanchard**[2]   **Manuel Melon**[2]
Laurent Simon[2]   **Kais Hassan**[2]   **Rozenn Nicol**[3]

[1] LMFA, UMR CNRS 5509, Lyon University, UCBL, ECL, INSA Lyon, 69134 Écully, France
[2] LAUM, UMR 6613, Institut d'Acoustique - Graduate School (IA-GS),
CNRS, Le Mans Université, France
[3] Orange Labs, 2 avenue Pierre Marzin, 22307 Lannion Cedex

`pierre.lecomte@univ-lyon1.fr`

ABSTRACT

Spherical microphone arrays are widespread nowadays, especially with the advent of techniques for decomposing acoustic fields on the basis of spherical harmonics (i.e. Ambisonics). In these approaches, the corresponding arrays require a quadratically increasing number of microphones as the degree of the components to be estimated increases. Besides, for some applications, it is unnecessary to represent the whole solid angle of the sound field from the array point of view: for instance as soon as the array is placed near the boundaries of the acoustic field of study (i.e. walls in a room). To tackle these issues, one proposes a geometry which uses the acoustic rigid boundary condition at room walls to decrease the number of required microphones. With one eighth of a sphere array placed in the corner of a room, only certain spherical harmonics are required for the sound pressure field decomposition, and the microphone number can drop up to 8 times lower when compared to the full spherical array configuration. A microphone array prototype having the geometry of one eighth of a sphere is described, built, and evaluated in a rigid bounded eighth of an anechoic space.

1. INTRODUCTION

Spherical Harmonics (SH) beamforming is a common technique for sound field analysis which rely on the sound pressure field decomposition onto the SHs basis with Spherical Microphone Arrays (SMA) [1]. This approach allows to steer a rotationnaly-invariant beampattern in the whole 4π steradian solid angle. However, in many situations, especially in rooms, not all these directions are useful for the sound field analysis. For instance, if the SMA is close to a room wall, all the acoustic sources lie in the same angular sector from the SMA point of view. In [2], an approach is proposed to consider only spherical fraction (SF) domains, bounded by rigid conditions to perform SF beamforming. It is shown that the sound pressure decomposition is done onto a sub-basis of SH, called the Spherical Fractions Harmonics (SFH). In this work, a spherical fraction domain of one eighth, bounded by rigid planes, is considered. A Spherical Fraction Microphone Array (SFMA) is designed and evaluated in one-eighth anechoic chamber. The paper is organized as follows: In Sec. 2, the SFH $Y_{l,m,1/8}$ for the eighth of a sphere are recalled. Then, the SF beamforming equations are presented in Sec. 3. In Sec. 4 the design of an SFMA with one eighth of a sphere geometry is described. Details on its building are given in Sec. 5. An experimental evaluation is carried out in Sec. 6. The results are presented in Sec. 7 and discussed in Sec. 8. The paper concludes in Sec. 9.

2. SPHERICAL FRACTION HARMONICS

In [2], the SFH are derived: It is a basis of orthonormal functions on a rigid-bounded fraction of the unit sphere, among one eighth-, a quarter- or a half-sphere. It is shown that the SFHs form sub-basis of SH. In the present work, one deals with one eighth of spherical domain rigid bounded with planes $x = 0$, $y = 0$ and $z = 0$ (gray planes on Fig. 1). The corresponding SFHs are denoted $Y_{l,m,1/8}$ and are defined by:

$$Y_{l,m,1/8}(\theta,\phi) = 2\sqrt{2}Y_{l,m}(\theta,\phi) \quad \text{for} \quad (l,m) \in \mathbb{M}_{1/8}. \tag{1}$$

In Eq. (1), $Y_{l,m}(\theta,\varphi)$ is the fully normalized SH of degree l and order m, evaluated at azimuth angle ϕ and polar angle θ. The set $\mathbb{M}_{1/8}$ is defined by:

$$\{(l,m) \in (\mathbb{N},\mathbb{Z}) \mid m \le l \wedge l \in 2\mathbb{N} \wedge m \in 2\mathbb{N}\}, \tag{2}$$

where the symbol $\wedge$ is the AND logical operator. From Eq. (2), it can be seen that there is no SFHs $Y_{l,m,1/8}$ for odd degree l. The SFHs $Y_{l,m,1/8}$ number up to degree L, denoted $Q(L)$ is given by:

$$Q_{1/8}(L) = \frac{1}{2}\left(\left\lfloor\frac{L}{2}\right\rfloor + 1\right)\left(\left\lfloor\frac{L}{2}\right\rfloor + 2\right). \tag{3}$$

The number $Q(L, 1/8)$ converges to 8 times less the number of SH, $(L+1)^2$ as L increases [2].

3. SPHERICAL FRACTION BEAMFORMING

3.1 Beamforming equations

Beamforming with SFH is shown to be similar to SH beamforming in [2]. As it is a modal beamforming, the sound pressure field is firstly decomposed onto the SFH basis with the Spherical Fraction Fourier Transform (SFFT), in order to obtain the components $\mathbf{b} \in \mathbb{C}^{Q(L)\times 1}$ up to

degree L. Then, these components are multiplied with the SFH weights according to a beampattern up to degree L and are summed to obtain the beamformer output [1]. These operations are given by:

$$y(\theta, \phi) = \mathbf{w}^T \mathbf{b}, \qquad (4)$$

where $y(\theta, \phi)$ is the beamformer output for a steering direction (θ, ϕ), $\mathbf{w} \in \mathbf{R}^{Q(L) \times 1}$ are the beampattern weights and ^{T} is the transpose operator. For a regular beamformer (i.e. plane wave decomposer [3]) with steering direction (θ, φ), the weights are given by [2]:

$$w_{l,m,1/8} = Y_{l,m,1/8}(\theta, \phi). \qquad (5)$$

Note that in case of SF beamforming, the regular beampattern described by Eq. (5) is not rotationnaly-invariant, as image beampatterns are generated due to the rigid domain boundaries. See [2] for more details.

3.2 Response to a plane wave

The SFHs components for a plane wave with Direction Of Arrival (DOA) (θ_s, ϕ_s) are given by:

$$b_{l,m,1/8} = Y_{l,m,1/8}(\theta_s, \varphi_s). \qquad (6)$$

4. MICROPHONE ARRAY DESIGN

In this section, the design of one eighth of a sphere SFMA is described.

4.1 Mesh construction

4.1.1 Gauss-Legendre cubature

For the prototype in the present work, the mesh is chosen starting from a Gauss-Legendre cubature rule at degree L [4, p. 66]. This weighted cubature rule can operate the Discrete Spherical Harmonics Transform (DSHT) up to a maximal degree L with no error. On the full sphere, the nodes are positioned with an equal-angle in azimuth ϕ, and at zenith angles θ corresponding to the zeroes of $P_{L+1}(\cos(\theta))$. Each node is weighted with the weight α_q. At degree L there are $N = 2(L+1)^2$ nodes on the full sphere. The node positions and weights are given by the following formulas:

$$\begin{cases} \phi_n = (n + \dfrac{1}{2})\dfrac{2\pi}{2L+2}, & n \in \{0, \cdots, 2L+1\} \\[2mm] P_{L+1}(\cos(\theta_q)) = 0, & q \in \{0, \cdots, L\} \\[2mm] \alpha_q = \dfrac{\pi}{L+1}\dfrac{2(1-\cos(\theta_q)^2)}{(L+2)^2(P_{L+2}(\cos(\theta_q))^2}, & q \in \{0, \cdots, L\} \end{cases} \qquad (7)$$

4.1.2 One eighth of spherical mesh

From Eq. (7), for an odd degree L, there are $L+1$ even number of roots for $P_{L+1}(\cos(\theta)) = 0$. The corresponding directions θ_q, are grouped by pair, symmetric to plane $z = 0$ without possibility of north and south poles direction. As well, there are an even number of azimuth directions ϕ_n which are symmetrical with respect to the $x = 0$ and $y = 0$ planes. Note that the starting angle for $n = 0$ in
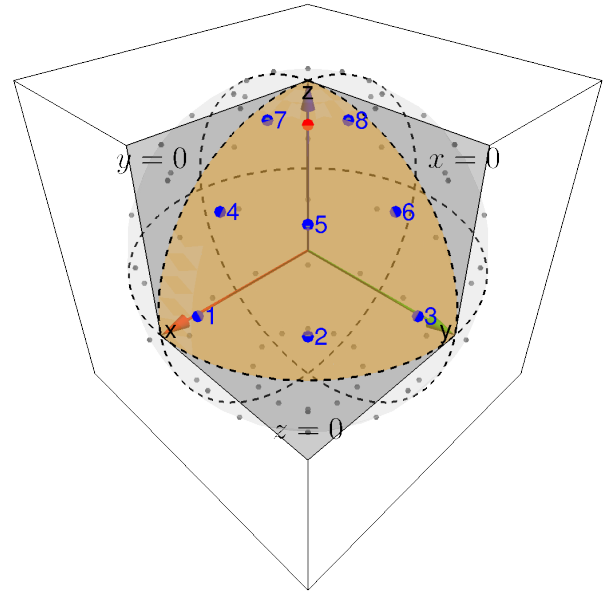
Figure 1: One eighth of a spherical Gauss-Legendre mesh for $L = 5$. The full sphere mesh is shown as the union of gray, blue and red nodes; the eighth of spherical mesh as the union of blue and red node. The mesh used for the SFMA prototype is shown in blue. The eigth of spherical fraction is shown in orange and the rigid bounding planes $x = 0$, $y = 0$ and $z = 0$ are shown in gray.

Eq. (7) ensures that no nodes will be on the planes $x = 0$ or $y = 0$, in order to facilitate the mounting of microphone during the prototype building. Finally, the resulting mesh presents symmetries with respect to plane $x = 0$, $y = 0$ and $z = 0$. From the full sphere mesh, by retaining only the nodes belonging to one eighth of a sphere, one eighth of a spherical mesh is obtained with a number of nodes $N_{1/8} = N/8$. According to the image source principle [5], this mesh is able to operate the Discrete Spherical Fraction Harmonics Transform (DSFHT) on a eighth of a sphere up to degree L. Note that the node weights α_q should be multiplied by 8 to ensure the orthonormality of $Y_{l,m,1/8}$. The full sphere mesh at degree $L = 5$ with $N = 72$ nodes is visible on Fig. 1 as the union of gray, blue and red nodes. The blue and red nodes only correspond to one eighth of a sphere mesh with $N_{1/8} = 9$ nodes. Note that other meshing strategies are possible, using an optimization algorithm as in [6] for instance.

4.1.3 Removing one node

A drawback of the Gauss-Legendre cubature is that it concentrates nodes close to the poles as it can be seen on Fig. 1. This can be cumbersome when making the prototype due to the size of the MEMS microphone Printed Circuit Board (PCB). Moreover, the sound card embedded inside the prototype allows to stream a maximum of 8 channels (see Sec 5.3). For these reasons, it was chosen to use a Gauss-Legendre quadrature up to $L = 5$, to take the eighth of the resulting spherical mesh, and to remove a node, shown in red in Fig.1. This gives a total of 8 nodes to integrate 6 SFHs $Y_{l,m,1/8}$. As a consequence,

the Gauss-Legendre cubature weights in the Eq. 7 can not be used anymore. The sound pressure projection DSFHT is then performed as follows:

$$\mathbf{p} = \mathbf{Y}^\dagger \mathbf{s}. \tag{8}$$

In Eq. (8), $\mathbf{s} \in \mathbb{C}^{N_{1/8} \times 1}$ are the sensors pressure signals, $\mathbf{Y} \in \mathbb{R}^{N_{1/8} \times Q_{1/8}(L)}$ is matrix containing the SFHs evaluated at the nodes directions up to degree L, $\mathbf{Y}^\dagger = (\mathbf{Y}^T \mathbf{Y})^{-1} \mathbf{Y}^T \in \mathbb{R}^{Q_{1/8}(L) \times N_{1/8}}$ is the Moore-Penrose pseudo-inverse of the $\mathbf{Y}$ and $\mathbf{p} \in \mathbb{R}^{Q(L) \times 1}$ are the DSFHT pressure coefficients. Note that this approach can be used as long as the number of nodes is greater or equal to $Q(L)$ [7].

4.1.4 Sound pressure field components estimation

After DSFHT operation, the components $\mathbf{p}$ are weighted with the following radial filters in the case of a rigid sphere configuration of radius a [8]:

$$E_l(ka) = i^{1-l}(ka)^2 h'_l(ka). \tag{9}$$

In Eq. (9), $i = \sqrt{-1}$, a is the array radius, $k = 2\pi f/c$ is the wave number with f the frequency and c the sound speed. The function h'_l is the first derivative, with respect to argument ka, of the spherical Hankel function of second kind. Note that such filters present excessive amplification at low frequencies and higher degree L. A regularized version, using the Thikhonov approach [7] is used in practice. The sound field components $\mathbf{b}$ are then obtained by:

$$\mathbf{b} = \mathbf{E}\mathbf{p}. \tag{10}$$

In Eq. (10), $\mathbf{E} \in \mathbb{R}^{Q(L) \times Q(L)}$ is a diagonal matrix with diagonal terms given by $E_l(ka)$.

4.2 Aliasing error analysis

During the Discrete Spherical Fraction Fourier Transform (DSFFT) of the sound pressure, spatial aliasing occurs [9]. The orthornomality error matrix is good indicator to assess the aliasing. This matrix is denoted $\mathbf{D}$ and it is given by [7, 8]:

$$\mathbf{D} = \mathbf{Y}^\dagger \mathbf{Y} - \mathbf{I}, \tag{11}$$

where, $\mathbf{D} \in \mathbb{R}^{Q(L) \times Q(L')}$ and $\mathbf{I} \in \mathbb{R}^{Q(L) \times Q(L')}$ is a matrix with ones on the diagonal and zeros elsewhere. The orthonormality error matrix for $L = 4$ and $L' = 10$ is shown on Fig. 2. From Fig. 2, it can be seen that the orthonormal-
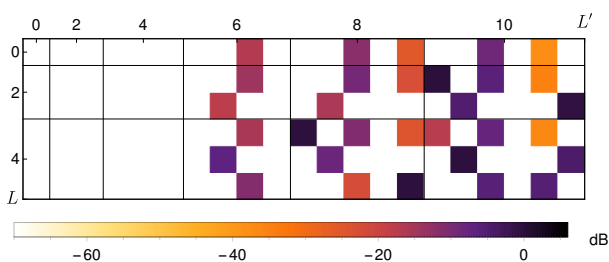
Figure 2: Orthonormality error matrix $\mathbf{D}$ for the proposed 8-node mesh.

ity error is negligible up to degree $L = 4$. Beyond that, errors are sometimes negligible, but some are high enough to bring spatial aliasing when estimating sound pressure field components using Eq. (10). Following [8, Eq. 46], the average aliasing error at capture for plane waves is plotted versus frequency for an array radius of $a = 0.1$ m in Fig. 3. For this plot, the orthonormality errors were taken into account up to degree $L' = 30$. From Fig. 3, it can be seen
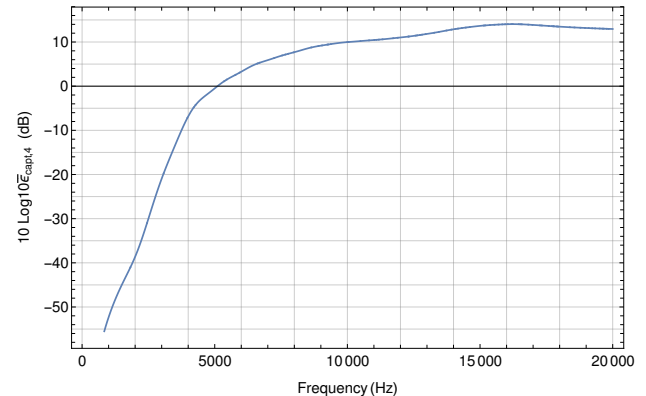
Figure 3: Average aliasing error at capture versus frequency for plane wave, for the proposed 8-node mesh.

that average aliasing error does increase with frequency. If one takes -3 dB as a maximum acceptable relative error, the corresponding aliasing frequency is $f_{\text{alias}} \simeq 4474$ Hz.

5. PROTOTYPE REALIZATION

In this section, the realization of a 0.1 m radius, one eighth of a sphere SFMA is described. The prototype is intended to be easy and low-cost to produce. The one eighth SF is made with 3D printing. The microphones used are digital Micro Electro-Mechanical System (MEMS) microphones, pre-soldered on PCB. The acquisition board is integrated to the assembly and connected to a computer by Universal Serial Bus (USB). The following sections describe these different elements in more detail.

5.1 3D Printing

A spherical shell design is chosen, to allow the inclusion, of all the microphone circuitry and the embedded acquisition card, in the prototype. It is realized by Fused Deposition Modeling (FDM) 3D-Printing in PolyLactic Acid (PLA) plastic. The shell is 15 mm thick with external radius $a = 0.1$ m. Its design on OpenScad[1] Computer-Aided Design (CAD) software is shown in Fig. 4a and the final printed shell is shown in Fig. 4b.
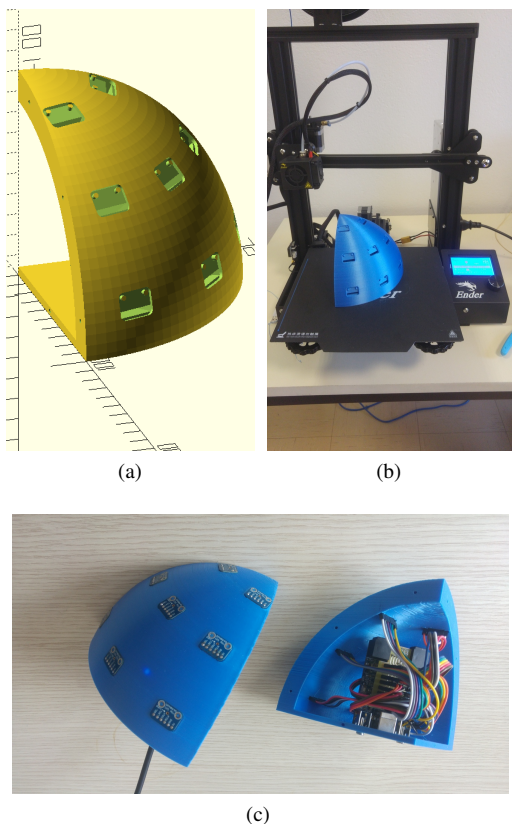
5.2 MEMS Microphones

The 8 microphones used for the prototype are Knowles SPH0645LM4H, Integrated Interchip Sound (I2S) protocol, omnidirectional digital MEMS.[2] They are pre-soldered on PCB, as evaluation boards manufactured by

---

[1] https://www.openscad.org/
[2] https://cdn-shop.adafruit.com/product-files/3421/i2S+Datasheet.PDF

Adafruit.[3] Each microphone PCB is clipped on the 3D printed shell, as shown on the left side of Fig. 4c. The wiring to the USB Streamer are done using Dupont prototype cable, as shown on the right side of Fig. 4c.
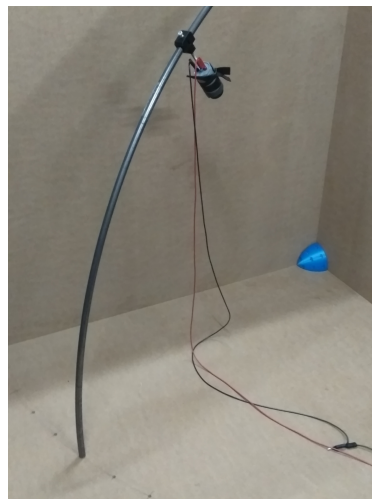

(a)　　　　　　　(b)

(c)

Figure 4: One eight of a sphere SFMA design and building. (a) Spherical shell design on OpensCAD software. (b) The spherical shell built using a FDM 3D printer. (c) The SFMA prototype with MEMS microphones and USB streamer embedded.

5.3 Embedded USB streamer

A Mini-DSP© USB Streamer Kit[4] is embedded inside the 3D printed shell. It is able to synchronize and stream up to 8 I2S MEMS microphone signals to the computer. It is visible on the right side of Fig. 4c. A custom-made PCB was used to easily connect the Dupont cable to the USB Streamer.

6. EXPERIMENTAL MEASUREMENTS

Once built, the prototype is tested in a rigid bounded eighth of space lying in an anechoic environment. It is mounted at the junction of three wooden panels of dimensions 2×2 m^2 in the LAUM anechoic room, as shown in Fig. 5. A metallic circular rod allows to place a 2-inches AuraSound loudspeaker at a radial distance of 1 m from the SFMA center and various angle of incidence. The loudspeaker is playing an exponential sweep sine from 200 Hz

[3] https://www.adafruit.com/product/3421
[4] https://www.minidsp.com/products/
usb-audio-interface/usbstreamer

Figure 5: Experimental layout: The SFMA is placed at the corner of 3 wooden panels mounted in a anechoic room. A loudspeaker can move on a eighth of a 1 m radius spherical surface, centered on the corner.

to 8 KHz in order to estimate the corresponding frequency responses on each SFMA microphone. Then, Eq. (8) and Eq. (10) are used to decompose the sound pressure field onto the SFH $Y_{l,m,1/8}$ basis.
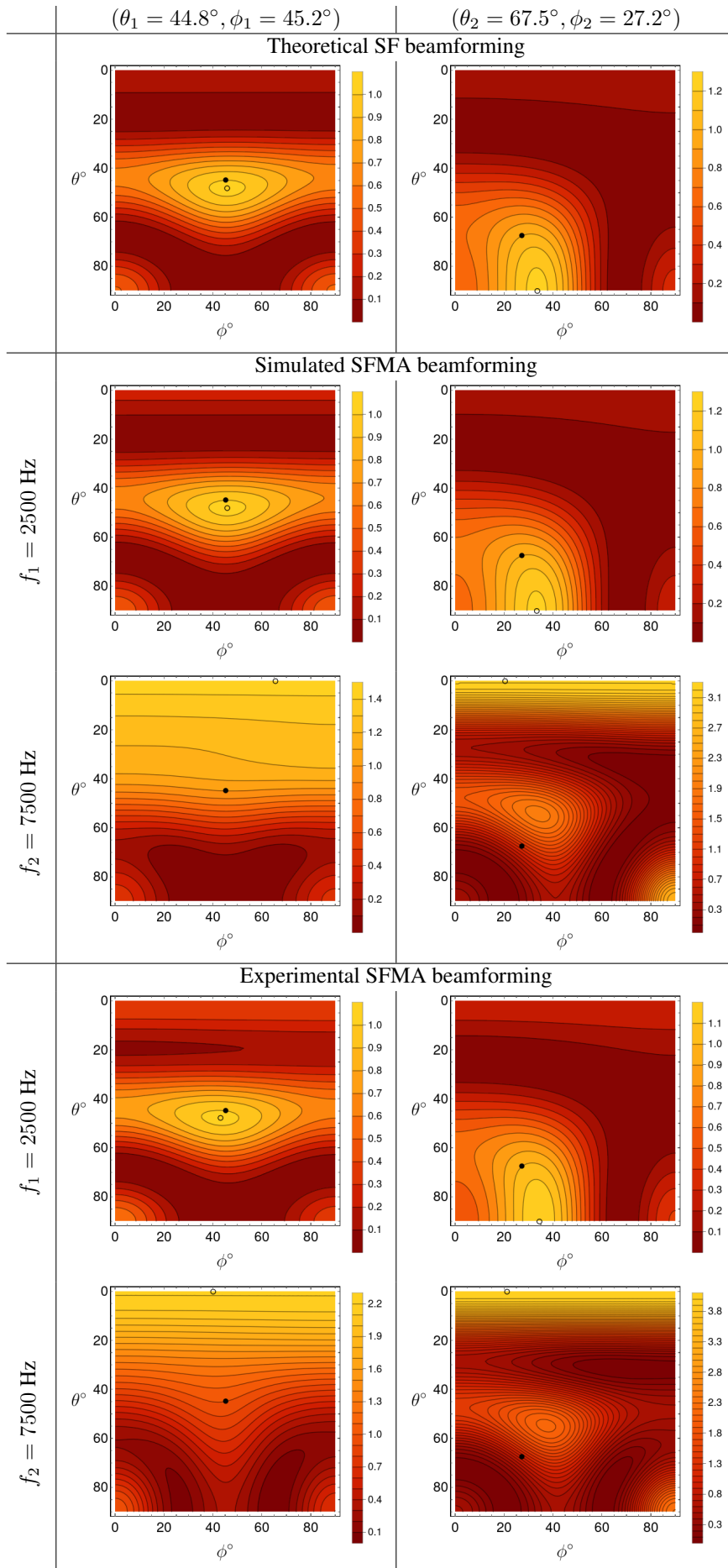
7. RESULTS

Two DOAs of the acoustic source and two frequencies are chosen for simulation and experimental results. The angles are $(\theta_1 = 44.8°, \phi_1 = 45.2°)$ and $(\theta_2 = 67.5°, \phi_2 = 27.2°)$ and the frequencies $f_1 = 2500$ Hz $< f_{\text{aliasing}}$ and $f_2 = 7500$ Hz$> f_{\text{alias}}$. The degree of decomposition is $L = 4$. The normalized squared beamformer output $|y(\theta, \phi)|^2/|y(\theta_{1,2}, \phi_{1,2})|^2$ is plotted for all possible steering directions $(\theta, \varphi) \in (0°, 90°) \times (0°, 90°)$. The results are shown in Fig. 6. In these figures, the sound source DOA is shown with a black dot. The maximum of the directivity map is shown with a circle. The first row corresponds to the theoretical SF beamforming situation, where the sound field components are those of a plane wave, according to Eq. (6). The second and third rows correspond to the theoretical results of the SFMA meshing proposed in Sec. 4, also for a plane wave. Finally, the fourth and fifth lines correspond to the experimental results of Sec. 6.

8. DISCUSSION

Theoretical beamforming For the theoretical beamforming situation, the results are independent of frequency. It can be observed that the direction of the maxima is not coincident with the the plane wave DOA. In particular, for the DOA (θ_2, ϕ_2) where the angular deviation is important. This result is expected as a limitation to work in a rigid-bounded SF domain. Indeed, image beampatterns, symmetric to the rigid boundary planes, are generated during the beamforming procedure and their superposition tends

Figure 6: Beamforming results for two sources DOA ($\theta_1 = 44.8°, \phi_1 = 45.2°$) and ($\theta_2 = 67.5°, \phi_2 = 27.2°$) and the frequencies $f_1 = 2500$ Hz and $f_2 = 7500$ Hz. The normalized squared beamformer output $|y(\theta, \phi)|^2/|y(\theta_{1,2}, \phi_{1,2})|^2$ is plotted for all possible steering directions $(\theta, \varphi) \in (0°, 90°) \times (0°, 90°)$.

to deflect the position of the SF resulting beampattern maximum. This phenomenon is studied in more detail in [2]. In particular, the SF beampattern can be seen as the sum of eight free-field beampatterns. The free field beampattern Full Width at Half Maximum (FWHM), denoted Θ, will govern the position of the resulting maxima. In particular, at degree $L = 4$, a free-field beampattern FWHM is around $\Theta \simeq 52°$. When the plane wave DOA $(\theta_{1,2}, \phi_{1,2})$ is at an angular distance of a rigid boundary $\leq \Theta/2$, the resulting maxima will snap on the boundary. This is the case for (θ_2, ϕ_2), on the first row, second column of Fig. 6. The reader is referred to [2] for more details on this phenomenon.

Simulated SFMA beamforming When a SFMA is used, spatial sampling introduces a spatial alasing phenomenon, as specified in Sec. 4.2. Compared to the theoretical situation, the results become frequency-dependent. For the frequency $f_1 < f_{\text{alias}}$, when the degree $L = 4$, aliasing is negligible, as can be seen in Fig. 3. Thus, similar results to the theoretical situation are found, as can be observed by comparing the second and first line of Fig. 6. However, for the frequency $f_2 > f_{\text{alias}}$, the sound pressure field components of degree $l > 4$ aliases strongly on the lower components (see Fig. 3). This results in the generation of side lobes, which, when added to their image, degrades strongly the results, as it can be observed when comparing the first and third rows of Fig. 6.

Experimental SFMA beamforming Comparing the fourth and fifth lines with the second and third lines of Fig. 6, it can be observed that the experimental results are very similar to those simulated for the SFMA, although the acoustic source used is not a plane wave, and the wooden walls may not be perfectly rigid. In particular, it is interesting to observe the similarity of the results for the frequency $f_2 > f_{\text{alias}}$, beyond the aliasing frequency.

9. CONCLUSION

In this work a geometry of a microphone array in one eighth of a sphere was presented. By inserting this device at the junction of three reflecting walls, it is possible to operate SF beamforming in an eighth fraction of a sphere. The proposed mesh allows with 8 microphones to make a SF beamforming up to the degree $L = 4$. An aliasing study has been done, a prototype has been realized and tested in experimental conditions. The results are in a good agreement with the theory. Future work aims at studying the behavior of SFMA in a real environment (living room).

10. REFERENCES

[1] J. Meyer and G. Elko, "A highly scalable spherical microphone array based on an orthonormal decomposition of the soundfield," in *IEEE International Conference on Acoustics, Speech, and Signal Processing*, vol. 2, pp. 1781–1784, IEEE, 2002.

[2] P. Lecomte, M. Melon, and L. Simon, "Spherical Fraction Beamforming," *IEEE Transactions on Acoustics, Speech, and Signal Processing (In Press)*, 2020.

[3] B. Rafaely, "Plane-wave decomposition of the sound field on a sphere by spherical convolution," *The Journal of the Acoustical Society of America*, vol. 116, no. 4, pp. 2149–2157, 2004.

[4] B. Rafaely, *Fundamentals of Spherical Array Processing*. Springer, second ed., 2019.

[5] Z. Li and R. Duraiswami, "Hemispherical microphone arrays for sound capture and beamforming," in *IEEE Workshop on Applications of Signal Processing to Audio and Acoustics*, pp. 106–109, IEEE, 2005.

[6] H. Pomberger and F. Pausch, "Design and evaluation of a spherical segment array with double cone," *Acta Acustica united with Acustica*, vol. 100, no. 5, pp. 921–927, 2014.

[7] S. Moreau, J. Daniel, and S. Bertet, "3d sound field recording with higher order ambisonics-objective measurements and validation of spherical microphone," in *Audio Engineering Society Convention 120*, (Paris), pp. 1–24, AES, 2006.

[8] P. Lecomte, P.-A. Gauthier, C. Langrenne, A. Berry, and A. Garcia, "A Fifty-Node Lebedev Grid and Its Applications to Ambisonics," *Journal of the Audio Engineering Society*, vol. 64, no. 11, pp. 868–881, 2016.

[9] B. Rafaely, B. Weiss, and E. Bachmat, "Spatial aliasing in spherical microphone arrays," *IEEE Transactions on Signal Processing*, vol. 55, no. 3, pp. 1003–1010, 2007.